Electroquasistatic Analysis of the Gas Insulated Line for the ITER Neutral Beam Injector

P. Bettini, R. Specogna, and F. Trevisan

Dip. di Ingegneria Elettrica, Gestionale e Meccanica, Università degli Studi di Udine IT33100, Italy

In this paper, we formulate an electroquasistatic problem according to the discrete geometric approach. As an application, the transient behavior of the gas insulated transmission line for the ITER neutral beam injector system is analyzed.

Index Terms—**Cell's method, discrete geometric approach, electroquasistatics, FIT, high voltage applications, ITER, NBI.**

I. Introduction

ITER [1] is an international research and development project with the aim to demonstrate the scientific and technological feasibility of fusion energy: it will allow the study of plasmas in conditions similar to those expected in a electricity-generating fusion power plant. ITER is designed to generate 500 MW of fusion power for extended periods of time, ten times more then the energy input needed to keep the plasma at the right temperature. A number of key technologies for fusion will be tested including the main systems (heating, control, diagnostic and remote maintenance) needed for a real fusion power plant. Four *additional heating and current drive* systems are under design: neutral beam injection systems, radio frequency systems, electron cyclotron systems and ion cyclotron systems.

In this framework, we deal with the neutral beam (NB) system [2], which consists of four main subsystems: injector (see Fig. 1), power supply and voltage distribution system, control and data acquisition system, and auxiliary system. Two heating and current drive injectors are needed to heat the plasma to temperature required for fusion born and to achieve steady state operations (up to 3600 s); each injector delivers a deuterium beam of 16.5 MW, with energy of 1 MeV. The power supply system feeds the neutral beam injector (NBI) by a gas insulated transmission line (GITL) with the inner electrode polarized at the negative potential of 1 MV dc [3].

Due to the peculiar operating conditions of the NB system and its challenging requirements, several electromagnetic, thermal and mechanical analyses are needed for most of the NB elements. To investigate the electroquasistatic (EQS) behavior of crucial elements of the NB system, we propose a discrete geometric approach (DGA) to solve axisymmetric EQS problems in the time domain. The DGA [4], which is akin to the finite integration technique (FIT) presented in [10] and [11] and alternative to the standard finite element (FE) formulations proposed in [12] and [13], has been applied to the EQS analysis of a specific section of the GITL of the NB system.

II. Discrete Geometric Approach for EQS

The geometry of our EQS problem is axisymmetric. Thus, we construct a primal cell complex $\mathcal{K}$ whose volumes v are solids obtained by the rotation of an angle ϕ of a plane triangular mesh around the symmetry axis z, of a cylindrical reference frame (r, ϕ, z) and origin O. Moreover, all the fields—the electric field, the electric displacement field, and the current density field—involved in the EQS problem lay in a radial plane r, z and they are invariant by rotation of the plane.

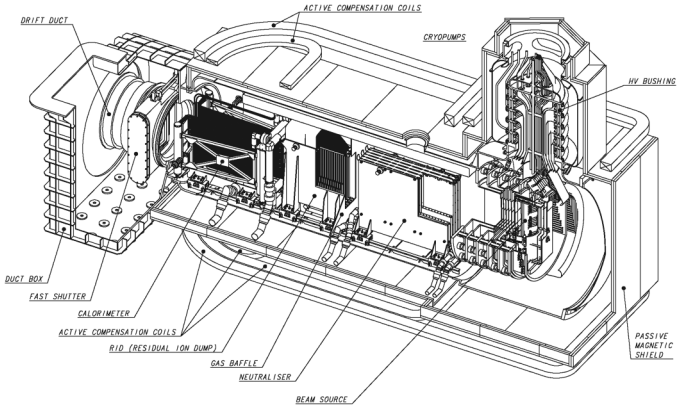

Fig. 1. Isometric view of the ITER neutral beam injector (NBI). Beam components (beam source, neutralizer, residual ion dump and calorimeter) are shown together with auxiliary components (cryopumps, HV bushing, drift duct, passive magnetic shielding, active compensation coils). The power supply system feeds the NBI by a gas insulated transmission line (GITL) connected to the HV bushing. Published with permission of ITER.

For clarity, we focus on the restriction of the primal complex to a single volume v, Fig. 2; we denote a primal node with n, a primal edge with e and a primal face with f. We construct the dual complex $\tilde{\mathcal{K}}$ according to the barycentric subdivision of $\mathcal{K}$ [4], [5]; thus the dual node $\tilde{n}$ is the center of mass of v, a dual edge $\tilde{e}$ is drawn from $\tilde{n}$ to the center of mass of f; a dual face $\tilde{f}$ and a dual volume $\tilde{v}$ are constructed as in Fig. 2.

The geometric elements of $\mathcal{K}$ and $\tilde{\mathcal{K}}$ are endowed with inner and outer orientations, respectively [5], [6]. The interconnections between the pairs (e, n), (f, e) of $\mathcal{K}$ are described by the incidence matrices $\mathbf{G}$, $\mathbf{C}$ respectively; we denote with $\tilde{\mathbf{D}}$ the incidence matrix between pairs $(\tilde{v}, \tilde{f})$ of $\tilde{\mathcal{K}}$ and $\tilde{\mathbf{D}} = -\mathbf{G}^T$ holds.

We consider the integrals of the field quantities involved in our EQS problem with respect to the oriented geometric elements of $\mathcal{K} - \tilde{\mathcal{K}}$, yielding the degrees of freedom (DoF) arrays. There is a precise association between the DoFs and the geometric elements of $\mathcal{K}$ and $\tilde{\mathcal{K}}$ [7], [8]. We denote with $\mathbf{U}$ the array of voltages associated with primal edges e, with $\mathbf{V}$ the array of scalar potentials associated with primal nodes n, with $\mathbf{Q}$ the array of electric charges associated with dual volumes $\tilde{v}$, with $\mathbf{I}$, $\mathbf{\Psi}$ the arrays of electric currents and electric fluxes across

Manuscript received October 07, 2008. Current version published February 19, 2009. Corresponding author: P. Bettini (e-mail: bettini@uniud.it).

Color versions of one or more of the figures in this paper are available online at http://ieeexplore.ieee.org.

Digital Object Identifier 10.1109/TMAG.2009.2012538

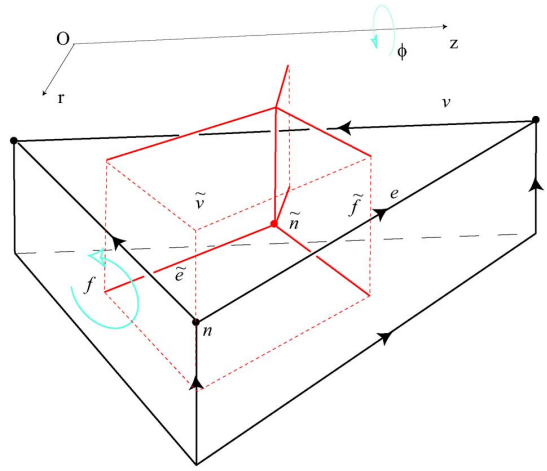

Fig. 2. A restriction of the primal and dual cell complexes is shown within a single volume v obtained by the rotation of a triangle in the plane of symmetry.

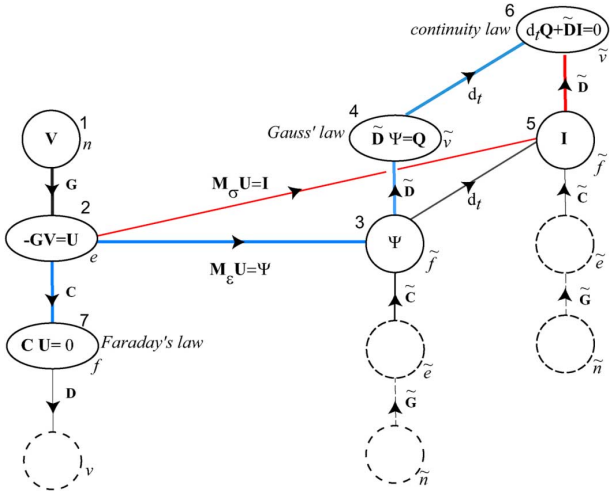

Fig. 3. Tonti's diagram for electroquasistatics. The incidence matrices $\mathbf{D}$, $\tilde{\mathbf{G}}$ and $\tilde{\mathbf{C}}$ are reported for completeness, even though they are not explicitly used in our formulation.

dual faces $\tilde{f}$. The DoFs arrays are regarded here as functions of a time instant.

A synthetic tool that gives relevance to the geometrical aspects of the approach, and allows to derive the algebraic equations of EQS, is the Tonti's diagram (for a comprehensive description, see [7]). Here, we derive it at a discrete level focusing on our EQS problem. On the right side of the diagram (Fig. 3) two vertical pillars are drawn, where each DoF-array[1] is associated with the corresponding geometric element of the dual cell complex (from nodes $\tilde{n}$ to volumes $\tilde{v}$, from bottom to top). On the left side of the diagram, only one of the two vertical pillars needs to be drawn for the case of EQS, where each DoF-array[2] is associated with the corresponding geometric element of the primal complex (from nodes n to volumes v, from top to bottom). The dashed circles represent categories of variables not used in this specific problem.

Along a vertical pillar, we move from the variables on one level to the variables on the successive level—for example from potentials $\mathbf{V}$ on nodes n to voltages $\mathbf{U}$ on edges e—of the primal or of the dual complex, using the incidence matrices. This process allows us to form, at each level, algebraic *balance* relations between variables of the same category—configuration or source—yielding the physical laws in discrete form: Faraday's law $\mathbf{CU} = 0$ which is identically satisfied by introducing a potential $\mathbf{V}$ such that $-\mathbf{GV} = \mathbf{U}$, Gauss' law $\tilde{\mathbf{D}}\mathbf{\Psi} = \mathbf{Q}$ and the continuity law $d_t\mathbf{Q} + \tilde{\mathbf{D}}\mathbf{I} = 0$, d_t being the time derivative.

The discrete counterparts of the constitutive relations are square matrices $\mathbf{M}_\varepsilon$, $\mathbf{M}_\sigma$ of dimension N (number of nodes of the triangular grid); they are represented as horizontal links from left to right. The electric constitutive matrix $\mathbf{M}_\varepsilon$ maps the array $\mathbf{U}$ to the array $\tilde{\mathbf{\Psi}}$, while Ohm's constitutive matrix maps the array $\mathbf{U}$ to the array $\mathbf{I}$; they can be constructed in different ways as described in [4], [9]–[11], [14]–[20] under the hypothesis of element-wise uniform fields and element-wise homogeneous permittivity and conductivity of the media. The diagram reveals that $\mathbf{M}_\varepsilon$, $\mathbf{M}_\sigma$ have the same geometric structure, since they map variables associated with primal edges e to variables associated with dual faces $\tilde{f}$, being in a one-to-one correspondence each other; this fact has a great impact on the implementation and on the coding economy: structurally $\mathbf{M}_\varepsilon$, $\mathbf{M}_\sigma$ coincide, provided that we swap permittivity with conductivity.

We can now derive the set of equations governing our EQS problem. By following in the diagram the path 1-2-3-4-6 and adding the addendum from the other path 1-2-5-6 (see Fig. 3), we obtain the differential system

$$\mathbf{K}_\epsilon d_t\mathbf{V} + \mathbf{K}_\sigma\mathbf{V} = 0 \tag{1}$$

where matrices $\mathbf{K}_\epsilon = \mathbf{G}^T\mathbf{M}_\epsilon\mathbf{G}$ and $\mathbf{K}_\sigma = \mathbf{G}^T\mathbf{M}_\sigma\mathbf{G}$ are constructed element by element and then assembled to yielding the global matrices, for code efficiency. The dual complex is constructed locally for each triangle separately; in this way its construction does not represent an overhead with respect to finite elements. Of course uniqueness is guaranteed by specifying proper initial and boundary conditions.

It should be noted that the matrix $\mathbf{K}_\epsilon$ is singular and to solve (1) we rely on an implicit Runge–Kutta method [21], [22]. Particularly, we considered the SDIRK subclass of IRK methods, where the coefficient matrix is lower triangular with one s-fold eigenvalue; SDIRKs are easier to implement than fully implicit ones (FIRKs) but they have a local order of at most 4, and they are called low order Runge–Kutta methods. However such orders are sufficient for the problem considered. An auxiliary Runge–Kutta method (together with the estimating one) is used for evaluating the local error and the pair of methods is often referred to as an *embedded pair*.

III. The EQS Problem

In the framework of ITER NB system design, alternative ion beam accelerator concepts were proposed by the EU and the JA Home Teams: SINGAP (single aperture, single gap) and MAMuG (multi-aperture, multi-gap), respectively [2].

In the SINGAP configuration, the GITL, which connects the power supply to the NBI, consists of two coaxial transmission lines (TL1, TL2), as shown in Fig. 4 [23]. The transmission lines are provided with two kinds of spacers: disk-shaped spacers and post spacers. Several tens of inner post spacers will be installed. On the other hand, the disk-shaped spacers will be used only when gas-tight barriers are needed, e.g. as interface with the paper–oil feedthrough and as TL1-HVD2 interface.

[1]These DoF-arrays are called *source* variables.

[2]These DoF-arrays are called *configuration* variables.

TABLE I
TRANSMISSION LINE SECTIONS (TL1, TL2)

	D_{int} [m]	D_{ext} [m]	E_{int} [kV/mm]	E_{ext} [kV/mm]
TL1	0.4	1.1	5.0	1.8
TL2	0.4	1.65	3.6	0.9

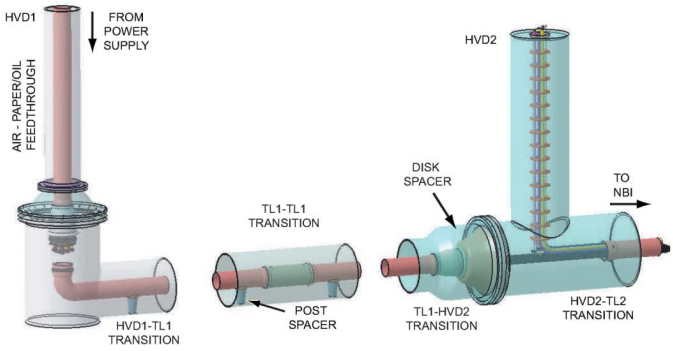

Fig. 4. Isometric view of the transmission lines (TL1, TL2) and their interfaces with the high voltage decks (HVD1, HVD2) for the SINGAP configuration of the NB system [23]. An inner post spacer and a disk spacer are also indicated.

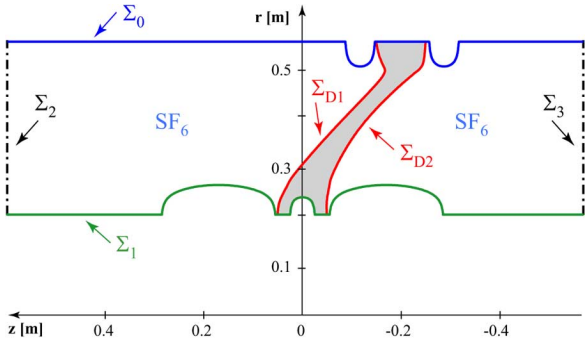

Fig. 5. Two-dimensional axisymmetric geometry of the simulated problem. Σ_{D1} and Σ_{D2} are the separation surfaces between the epoxy resin disk spacer and the SF_6 gas. Σ_1 and Σ_0 denote the internal and external (grounded) electrodes, respectively. Finally on Σ_2, Σ_3 the Neumann boundary condition is imposed.

The dimensions (internal (D_{int}), external (D_{ext}) diameters) of the coaxial conductor transmission lines and the nominal electric fields[3] are presented in Table I.

The insulation structure of the GITL for the SINGAP configuration has been designed taking into account operating conditions quite different from standard ac operation at power frequency [24]. In fact, the voltage applied between the electrodes of the GITL is approximately a square wave (-1 MV for 1000 s every hour), but transient over voltages will seldom occur depending on misoperation of the power supply; furthermore, the voltage frequently drops due to breakdowns across the accelerating gap and recovers in few tens of milliseconds.

In this paper we focus on EQS behavior of a specific section of the GITL, where an epoxy resin disk spacer is installed as gas (SF_6) tight barrier. A detail of the 2-D axisymmetric geometry of the simulated problem is shown in Fig. 5. The shape of the disk spacer and of the metallic screens on internal (Σ_1) and external (Σ_2) electrodes comes from the optimization procedure described in [24].

[3]Nominal electric fields at internal (E_{int}), external (E_{ext}) electrodes are referred to 1 MV dc, SF_6 pressure of 0.3 MPa, pure cylindrical geometry.

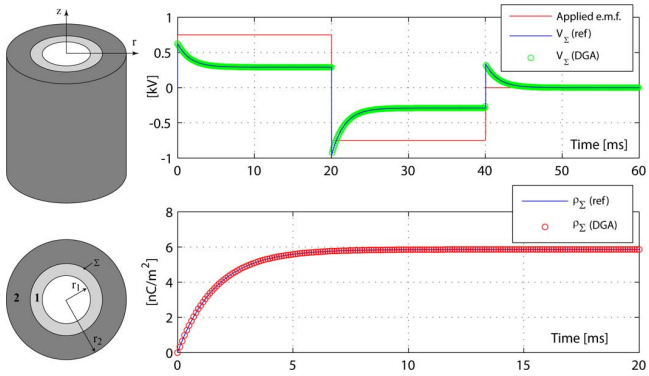

Fig. 6. On the left side: Isometric view and cross section of the Maxwell cylindrical capacitor. On the right side, top to bottom: Applied e.m.f. and time evolution of the electric potential V_Σ of the interface surface Σ; time evolution of the electric charge density ρ_Σ.

The proposed approach allows to study, in particular, a critical issue: the electric charge density stored on the separation surfaces between gas and solid insulator $(\Sigma_{D1}, \Sigma_{D2})$ during the evolution of the electric field when a reference voltage waveform is applied between Σ_1 and Σ_0 electrodes.[4]

IV. NUMERICAL RESULTS

In order to assess the EQS solver, we consider first the benchmark case of the so-called Maxwell capacitor. Then, we will proceed with the simulation of the disk-shaped spacer.

A. Maxwell Capacitor Benchmark

The Maxwell capacitor has been considered as an axisymmetric benchmark problem; it consists of two cylindrical electrodes ($r_1 = 4$ m, $r_2 = 10$ m, see Fig. 6, left), separated by two dielectric slabs ($\Delta_{r1} = 2$ m, $\Delta_{r2} = 4$ m). As material parameters, relative permittivity $\epsilon_1 = 4$, $\epsilon_2 = 1$ and electric conductivity $\sigma_1 = 10^{-8}$ S/m, $\sigma_2 = 2 \cdot 10^{-8}$ S/m are assumed. An e.m.f. has been applied between the electrodes, with two voltage steps (at $t_1 = 20$ ms and $t_2 = 40$ ms, with a rise/fall time $\Delta t = 10\ \mu$s).

The time evolution of the electric potential V_Σ of the interface surface Σ is presented in Fig. 6, right (top). An excellent agreement is shown between the numerical results calculated by DGA (2300 elements, 1200 DoFs) and the analytical reference values. The time evolution of the electric charge density ρ_Σ, calculated by DGA, is compared to the analytical solution in Fig. 6, right (bottom), from $t = 0$ s (*capacitive* field distribution) to $t = 20$ ms (*resistive*—steady state—field distribution). The transient behavior is controlled by a time constant

$$\tau = \varepsilon_0 \cdot \frac{\varepsilon_1 \log(r_2/r_\sigma) + \varepsilon_2 \log(r_\sigma/r_1)}{\sigma_1 \log(r_2/r_\sigma) + \sigma_2 \log(r_\sigma/r_1)} = 1.64 \text{ ms}.$$

B. GITL Simulation

In the numerical simulations of the 2-D axisymmetric domain (Fig. 5), the boundary conditions are assigned to close the problem, by prescribing the e.m.f. $u(t)$ applied between Σ_1 and Σ_0, and zero electric flux condition on Σ_2,

[4]In fact, the minimization of the surface charge density has been proven [25] to be effective in increasing the long-term voltage stability of the epoxy-SF_6 interface.

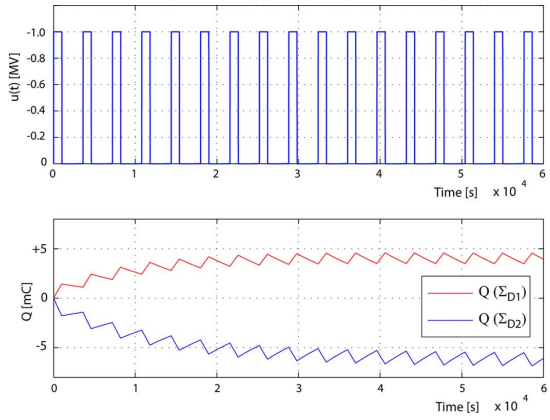

Fig. 7. Top: square voltage waveform $u(t)$ applied between Σ_1 and Σ_0. Bottom: time evolution of the electric charge stored on Σ_{D1} and Σ_{D2}.

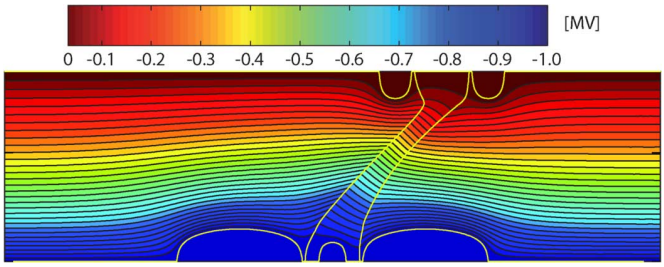

Fig. 8. Electric field distribution (equipotential lines) calculated by DGA towards the end of the EQS simulation ($t = 58\,600$ s).

Σ_3. As material parameters, relative permittivity $\epsilon_{\text{epoxy}} = 4$, $\epsilon_{SF_6} = 1$, and electric conductivity $\sigma_{\text{epoxy}} = 3.5 \cdot 10^{-15}$ S/m, $\sigma_{SF_6} = 2 \cdot 10^{-20}$ S/m are assumed [24].

In Fig. 7 the applied voltage $u(t)$ (square wave with amplitude $V_M = -1$ MV, period $T = 3600$ s, duty cycle $\delta = 0.28$) is presented, together with the time evolution of the electric charge stored on Σ_{D1}, Σ_{D2}, calculated by DGA, between $t = 0$ s and $t = 61\,200$ s.

The DGA code, developed in Fortran 90, takes less than 15 min to perform the EQS simulation with a maximum time step of 50 s on a laptop with a P4 2.4 GHz processor, 2 GB RAM. The computational time also includes the mesh generation (26 894 triangular cells, 13 716 nodes), the assembling of the stiffness matrices and the post-processing stage for all time steps (including the data storage on hard disk).

The electric field distribution (equipotential lines) calculated by DGA towards the end of the EQS simulation ($t = 58\,600$ s), the electric charge stored on each surface having reached the maximum value, is presented in Fig. 8.

V. Conclusion

The reformulation in terms of the discrete geometric approach of an electroquasistatic problem has been presented and applied to simulation of a peculiar section of the high-voltage transmission line of the neutral beam system of ITER experiment for fusion research. First, we validated the developed code on a reference axisymmetric electroquasistatic problem based on the so-called Maxwell capacitor; the obtained numerical results matched the analytical solution with great accuracy. Then the operating square voltage waveform was applied to the case of the gas-insulated transmission line of the neutral beam system of ITER and the corresponding numerical results were presented.

References

[1] R. Aymar, "ITER R&D: Executive summary: Design overview," *Fusion Eng. Des.*, vol. 55, no. 2–3, pp. 107–118, 2001.
[2] T. Inoue, R. Hemsworth, V. Kulygin, and Y. Okumura, "ITER R&D: Auxiliary systems: Neutral beam heating and current drive system," *Fusion Eng. Des.*, vol. 55, no. 2–3, pp. 291–301, 2001.
[3] K. Watanabe *et al.*, "Development of a dc 1 MV power supply technology for NB injectors," *Nucl. Fusion*, vol. 46, pp. S332–S339, 2006.
[4] E. Tonti, "Finite formulation of the electromagnetic field," *IEEE Trans. Magn.*, vol. 38, no. 2, pp. 333–336, 2002.
[5] A. Bossavit and L. Kettunen, "Yee-like schemes on staggered cellular grids: A synthesis between FIT and FEM approaches," *IEEE Trans. Magn.*, vol. 36, pp. 861–867, 2000.
[6] E. Tonti, "Algebraic topology and computational electromagnetism," in *Proc. 4th Int. Workshop on Electric and Magnetic Fields*, Marseille, France, May 12–15, 1988, pp. 284–294.
[7] E. Tonti, "On the formal structure of physical theories," in *Quaderni dei Gruppi di Ricerca Matematica del CNR*, 1975.
[8] E. Tonti, "On the geometrical structure of elecromagnetism," in *Gravitation, Electromagnetism and Geometrical Structures, for the 80th Birthday of A. Lichnerowicz*, G. Ferrarese, Ed. Bologna, Italy: Pitagora Editrice, 1995, pp. 281–308.
[9] T. Tarhasaari, L. Kettunen, and A. Bossavit, "Some realizations of a discrete Hodge operator: A reinterpretation of finite elements techniques," *IEEE Trans. Magn.*, vol. 55, no. 3, pp. 1494–1497, 1999.
[10] M. Clemens *et al.*, "Transient electro-quasistatic adaptive simulation schemes," *IEEE Trans. Magn.*, vol. 240, no. 2, pp. 1294–1297, 2004.
[11] T. Steinmetz *et al.*, "Electro-quasistatic field simulations based on a discrete electromagnetism formulation," *IEEE Trans. Magn.*, vol. 42, no. 4, pp. 755–758, 2006.
[12] A. Kurita, E. Takahashi, J. Ozawa, M. Watanabe, and K. Okuyama, "DC flashover voltage characteristics and their calculation method for oil-immersed insulation systems in HVDC transformators," *IEEE Trans. Power Delivery*, vol. PWRD-1, no. 3, pp. 184–190, 1986.
[13] K. Preis, O. Bíró, P. Supancic, and I. Ticar, "FEM simulation of thermistors including dielectric effects," *IEEE Trans. Magn.*, vol. 39, no. 3, pp. 1733–1736, 2003.
[14] P. Bettini and F. Trevisan, "Electrostatic analysis for plane problems with finite formulation," *IEEE Trans. Magn.*, vol. 39, no. 3, pp. 1127–1130, 2003.
[15] F. Bellina, P. Bettini, E. Tonti, and F. Trevisan, "Finite formulation for the solution of a 2-D eddy-current problem," *IEEE Trans. Magn.*, vol. 38, no. 2, pp. 561–564, 2002.
[16] M. Marrone, "A new consistent way to build symmetric constitutive matrices on general 2-D grids," *IEEE Trans. Magn.*, vol. 40, no. 2, pp. 1420–1423, 2004.
[17] L. Codecasa, R. Specogna, and F. Trevisan, "Symmetric positive-definite costitutive matrices for discrete eddy-current problems," *IEEE Trans. Magn.*, vol. 42, no. 2, pp. 510–515, 2007.
[18] M. Clemens and T. Weiland, "Discrete electromagnetism with the finite integration technique," in *PIER 32*, F. L. Teixeira, Ed. Cambridge, MA: EMW Pub., 2001, pp. 65–87.
[19] R. Specogna and F. Trevisan, "Discrete constitutive equations in $A - \chi$ geometric eddy-currents formulation," *IEEE Trans. Magn.*, vol. 41, no. 4, pp. 1259–1263, Apr. 2005.
[20] F. Trevisan, "3-D eddy current analysis with the cell method for NDE problems," *IEEE Trans. Magn.*, vol. 40, no. 2, pp. 1314–1317, 2004.
[21] F. Cameron, M. Palmroth, and R. Piché, "Quasi stage order conditions for SDIRK methods," *Appl. Numer. Math.*, vol. 42–41, pp. 61–75, 2002.
[22] F. Cameron, R. Piché, and K. Forsman, "Variable step size time integration methods for transient eddy current problems," *IEEE Trans. Magn.*, vol. 34, no. 5, pp. 3319–3322, 1998.
[23] V. Antoni, "The ITER neutral beam system: Status of the project and review of the main technological issues," presented at the 24th Symp. Fusion Technology, Warsaw, Poland, Sep. 11–15, 2006.
[24] A. De Lorenzi, L. Grando, R. Gobbo, G. Pesavento, P. Bettini, R. Specogna, and F. Trevisan, "The insulation structure of the 1 megavolt transmission line for the ITER neutral beam injector," *Fusion Eng. Des.*, vol. 82, pp. 836–844, 2007.
[25] E. Volpov, "HVDC gas insulated apparatus: Electric field specificity and insulation design concept," *IEEE Electr. Insul.*, vol. 18, no. 2, pp. 7–14, 2002.